

Coherent treatment of the self-consistency and the environment-dependency in a semi-empirical Hamiltonian: Applications to bulk silicon, silicon surfaces, and silicon clusters

C. Leahy, M. Yu, C. S. Jayanthi, and S. Y. Wu

Department of Physics, University of Louisville, Louisville, Kentucky 40292, USA

(Received 25 October 2005; revised manuscript received 5 June 2006; published 5 October 2006)

The key to the construction of *reliable* and *transferable* semiempirical Hamiltonians for quantum mechanics-based simulations of materials is to capture the effect of screening by electrons for different condensed phases of materials. In the present work, this objective is achieved through the development of a scheme for constructing a self-consistent (SC) and environment-dependent (ED) multicenter Hamiltonian in the framework of linear combination of atomic orbitals (LCAO) that involves careful modeling and optimization of parameters for electron-electron correlations and multicenter interactions. As an illustration of our method, we have used this scheme to construct the SCED/LCAO Hamiltonian for silicon. The robustness of this Hamiltonian is demonstrated by scrutinizing the properties of both bulk silicon and other complex structures of silicon with reduced symmetries. In particular, we have studied the following: (i) the binding energy versus relative atomic volume of different phases of bulk silicon, (ii) the stable structure of an intermediate-size Si_{71} cluster, (iii) the reconstruction of Si(100) surface, and (iv) the energy landscape for a silicon monomer adsorbed on the reconstructed Si(111)- 7×7 surface. The success of the SCED/LCAO Hamiltonian in the above applications, where silicon exists in a variety of different coordinations, is a testament to the predictive power of the scheme.

DOI: [10.1103/PhysRevB.74.155408](https://doi.org/10.1103/PhysRevB.74.155408)

PACS number(s): 73.22.-f, 68.35.Bs, 71.15.-m, 71.15.Ap

I. INTRODUCTION

Materials simulations based on total energy calculations and molecular dynamics (MD) using either the density functional theory (DFT) or tight-binding (TB) methods play central roles in the prediction of structural and system properties of complex materials. Both these methods have their respective advantages and disadvantages. For example, while DFT-based molecular dynamics (MD) schemes for the determination of structural properties of materials are expected to have predictive power, their applications are still limited to systems of about a few hundreds of atoms. On the other hand, TB-MD schemes are fast and applicable to larger systems. However, the transferability of conventional TB Hamiltonians is limited because they include only two-center interactions and they have no framework to allow the self-consistent determination of the charge redistribution. Hence they do not have the predictive power and can only be used, in the strictest sense, to provide explanation for system-specific experimental results.

In recent years, various schemes have been proposed to improve the transferability of TB Hamiltonians by including the self-consistency and/or the environment dependency.¹⁻¹¹ Among these schemes some are more readily amenable to MD simulation compared to others because of the ease with which atomic forces can be evaluated. These methods fall into two categories. While the emphasis of methods in one category is placed on a phenomenological description of the environment dependency,^{2,3} the framework of methods in the other category takes into account the self-consistency as well as the environment dependency.^{8,11}

The approach of Esfarjani and Kawazoe in Ref. 8 and that of Fraunheim *et al.* in Ref. 11 are very similar. For example, the approach in Ref. 11 is based on the expansion of the DFT-total energy in terms of the charge density fluctuations

about some reference density. To the second order in the density fluctuations,¹² the total energy is approximated as the sum of a band structure term and a short-range repulsive term corresponding to the conventional two-center TB Hamiltonian, plus a term representing the Coulomb interaction between charge fluctuations. Within this framework, the charge fluctuations can be self-consistently determined by solving an eigenvalue equation with the two-center Hamiltonian modified by a term that depends on the charge redistribution. While the Hamiltonian so defined does contain the features of self-consistency in the charge redistribution and the environment dependency for systems with charge fluctuations, the environment-dependent feature disappears when systems under consideration do not involve charge fluctuations, e.g., periodic extended systems containing one atomic species per unit cell. But the environment dependency is a key feature in a realistic modeling of the screening effect of the electrons in an aggregate of atoms, including extended periodic systems. This deficiency in properly mimicking the screening of the electrons can be critical in the development of a truly transferable Hamiltonian. Furthermore, in the approach of Ref. 11, the construction of the Hamiltonian and the determination of the total energy are, on the one hand, dependent on an optimal basis set of confined atomic orbitals obtained by solving a modified Schrödinger equation for a free atom in the framework of a self-consistent local density approximation with the correction of the generalized gradient approximation (SC-LDA/GGA). In this way, the Hamiltonian and overlap matrix elements are determined as functions of the distance between pairs of atoms and then tabulated for extrapolation. On the other hand, the key terms in the correction to the charge fluctuations in the Hamiltonian and in the total energy expression are approximated using exponentially decaying spherical charge densities. These two approximations used in the scheme are therefore independent

and unrelated. Hence, although the scheme proposed in Ref. 11 is parameter free, it may not be sufficiently flexible to yield a Hamiltonian with a wide range of transferability (see discussions in Sec. II).

In the present work, we present a scheme for constructing *reliable* and *transferable* LCAO-based semiempirical Hamiltonians for quantum-mechanics based simulations of materials. In this scheme, the effect of screening by electrons is captured through a careful modeling of environment-dependent (ED) multicenter terms and electron-electron correlations that includes a self-consistent (SC) determination of charge redistributions. A semiempirical route is chosen for the construction of the system Hamiltonian not only because a semiempirical Hamiltonian allows the simulation for large systems but, more importantly, its framework has the flexibility to allow the database to provide the necessary ingredients for fitting parameters to capture the effect of electron screening. The scheme developed for the construction of self-consistent and environment-dependent LCAO Hamiltonians is general and can be applied to both elemental (metal or semiconductors) and compound systems. In the following, as a test case, we employ our scheme to construct the SCED-LCAO Hamiltonian for silicon. The transferability and the reliability of this Hamiltonian is demonstrated by applying it to different situations, including different phases of the bulk silicon, an intermediate-size silicon cluster (Si₇₁), and the energetics of Si adatoms adsorbed on the Si(111)-7×7. These examples will test the robustness of the SCED-LCAO Hamiltonian for silicon in 0-, 2-, and 3-dimensional (D) structures with different coordinations and symmetries. In a forthcoming paper (a sequel to the present one), the SCED-LCAO Hamiltonian will be used to study the relative stability of 1D Si nanowire (NW) structures. Preliminary results from this work have already been reported in Ref. 40, where an excellent agreement between SCED-LCAO results and DFT-based VASP calculations have been found for Si NWs up to ~4 nm diameters.

The present paper is organized as follows. In Sec. II, our scheme for the construction of the SCED-LCAO Hamiltonian is delineated, with special emphasis placed on the parametric functions used to model the electron-electron correlation and multicenter interactions, where the parameters are obtained by fitting them to the structural and electronic properties of the bulk and clusters using an optimization procedure. In Sec. III, the robustness and the predictive power of the SCED-LCAO Hamiltonian is demonstrated for the following cases: (i) Structural properties of Si₇₁ cluster, (ii) reconstruction of Si(100) surface, and (iii) stable sites of adsorption for silicon monomer on Si(111)-7×7 surface. These case studies have been chosen to demonstrate the transferability, the reliability, the efficiency, and the predictive power of the SCED-LCAO Hamiltonian for complex Si-based structures with no or reduced symmetry. Section IV contains concluding remarks, computational efficiency, and future outlook of the SCED-LCAO scheme. Finally, the Appendix presents a brief outline of the optimization procedure used to determine the parameters of the SCED-LCAO Hamiltonian.

II. METHODOLOGY

A. SCED-LCAO Hamiltonian

In the framework of a semiempirical LCAO-based approach, the Hamiltonian is defined in terms of parametrized matrix elements $H_{i\alpha,j\beta}(\vec{R}_{ij})$ in some finite set of basis functions $\{\phi_{i\alpha}(\vec{r})\}$ not explicitly stated, where $i\alpha$ denotes the α orbital at the site i , and $\vec{R}_{ij} = \vec{R}_j - \vec{R}_i$ gives the relative position of the j th site with respect to the i th site. Within this context, the eigenvector c_λ , defining the coefficient vector of the expansion of the eigenfunction ψ_λ in terms of $\{\phi_{i\alpha}(\vec{r})\}$, satisfies a general eigenvalue equation

$$Hc_\lambda = E_\lambda S c_\lambda \quad (1)$$

with $S_{i\alpha,j\beta}(\vec{R}_{ij})$, the overlap matrix elements, being parametrized functions of R_{ij} within the framework of the basis functions $\{\phi_{i\alpha}(\vec{r})\}$. Our strategy for developing a general scheme to construct a reliable and transferable SCED-LCAO Hamiltonian for materials with predictive power is given as follows:

The Hamiltonian of an aggregate of many-atom may be written as

$$H = - \sum_i \frac{\hbar^2}{2m} \nabla_i^2 + \sum_{l,i} v(\vec{r}_l - \vec{R}_i) + \sum_{l,l'} \frac{e^2}{4\pi\epsilon_0 r_{ll'}} + \sum_{i,j} \frac{Z_i Z_j e^2}{4\pi\epsilon_0 R_{ij}}, \quad (2)$$

where $r_{ll'} = |\vec{r}_l - \vec{r}_{l'}|$, $R_{ij} = |\vec{R}_i - \vec{R}_j|$, $v(\vec{r}_l - \vec{R}_i)$ is the potential energy between an electron at \vec{r}_l and the ion at \vec{R}_i , Z_i the number of valence electrons associated with the ion at site \vec{R}_i , and the summation over l and l' runs over all the valence electrons. Within the one particle approximation in the framework of linear combination of atomic orbitals, the on-site (diagonal) element of the Hamiltonian can be written as

$$H_{i\alpha,i\alpha} = \epsilon_{i\alpha}^0 + u_{i\alpha}^{\text{intra}} + u_{i\alpha}^{\text{inter}} + v_{i\alpha}, \quad (3)$$

where $\epsilon_{i\alpha}^0$ denotes the sum of the kinetic energy and the energy of interaction with its own ionic core of an electron in the orbital $i\alpha$. The terms $u_{i\alpha}^{\text{intra}}$ and $u_{i\alpha}^{\text{inter}}$ are the energies of interaction of the electron in orbital $i\alpha$ with other electrons associated with the same site i and with other electrons in orbital $j\beta$ ($j \neq i$), respectively. The term $v_{i\alpha}$ represents the interaction energy between the electron in orbital α at site i and the ions at the other sites. In our scheme, the terms in Eq. (3) are represented by

$$\epsilon_{i\alpha}^0 = \epsilon_{i\alpha} - Z_i U_i, \quad (4)$$

$$u_{i\alpha}^{\text{intra}} = N_i U_i, \quad (5)$$

and

$$u_{i\alpha}^{\text{inter}} + v_{i\alpha} = \sum_{k \neq i} [N_k V_N(R_{ik}) - Z_k V_Z(R_{ik})], \quad (6)$$

where $\epsilon_{i\alpha}$ may be construed as the energy of the orbital α for the isolated atom at i , Z_i the number of positive charges carried by the ion at i (also the number of valence electrons associated with the isolated atom at i), N_i the number of

valence electrons associated with the atom at i when the atom is in the aggregate, U_i , a Hubbard-like term, the effective energy of electron-electron interaction for electrons associated with the atom at site i , $N_k V_N(R_{ik})$ the effective energy of interaction between an electron associated with an atom at site i and electrons associated with an atom at k , and $Z_k V_Z(R_{ik})$ the effective energy of interaction between an electron associated with an atom at i and an ion at site k . In our approach, $\varepsilon_{i\alpha}$ may be chosen according to its estimated value based on the orbital $i\alpha$, or treated as a parameter of optimization. The quantity U_i will be treated as a parameter of optimization while $V_N(R_{ik})$ and $V_Z(R_{ik})$ will be treated as parametrized functions to be optimized. An examination of Eqs. (3)–(6) clearly indicates that the presence of N_i , the charge distribution at site i , in the Hamiltonian provides the framework for a self-consistent determination of the charge distribution.

Following the same reasoning, we can set up the off-diagonal matrix element $H_{i\alpha,j\beta}$ ($j \neq i$) as

$$H_{i\alpha,j\beta} = \frac{1}{2} \left\{ K(R_{ij})(\varepsilon'_{i\alpha} + \varepsilon'_{j\beta}) + [(N_i - Z_i) + (N_j - Z_j)]U_i + \left[\sum_{k \neq i} (N_k V_N(R_{ik}) - Z_k V_Z(R_{ik})) + \sum_{k \neq j} (N_k V_N(R_{jk}) - Z_k V_Z(R_{jk})) \right] \right\} S_{i\alpha,j\beta}(R_{ij}). \quad (7)$$

Thus, in addition to the conventional two-center hopping-like first term, Eq. (7) also includes both intra- and inter-electron-electron interaction terms as well as environment-dependent multicenter (three-center explicitly and four-center implicitly) interactions. From Eq. (7), it can be seen that the environment-dependent multicenter interactions are critically dependent on $V_N(R_{ik})$ and $V_Z(R_{ik})$, in particular their difference $\Delta V_N(R_{ik}) = V_N(R_{ik}) - V_Z(R_{ik})$. Since $V_Z(R_{ik})$ is defined as the energy of effective interaction per ionic charge between an ion at site k and an electron associated with the atom at site i , we may model $V_Z(R_{ik})$ by the following parametrized function

$$V_Z(R_{ik}) = \frac{E_0}{R_{ik}} \{1 - (1 + B_Z R_{ik})e^{-\alpha_Z R_{ik}}\}, \quad (8)$$

where

$$E_0 = \frac{e^2}{4\pi\varepsilon_0}. \quad (9)$$

As both $V_N(R_{ik})$ and $V_Z(R_{ik})$ must approach E_0/R_{ik} for R_{ik} beyond a few nearest neighbor separations, $\Delta V_N(R_{ik})$ is expected to be a short ranged function of R_{ik} . We chose to model this short-ranged function by

$$\Delta V_N = (A_N + B_N R_{ik}) \frac{[1 + e^{-\alpha_N d_N}]}{[1 + e^{-\alpha_N (d_N - R_{ik})}]} \quad (10)$$

on account of the flexibility of the expression given in Eq. (10). Since $V_N(R_{ik}) \rightarrow U_i$ as $R_{ik} \rightarrow 0$, Eqs. (8) and (10) then leads to

$$A_N = U_i - (\alpha_Z - B_Z)E_0. \quad (11)$$

In its broadest sense, the first term in Eq. (7) corresponds to the Wolfsberg-Helmholtz relation in the extended Hückel theory.¹³ We modeled the scaling function K as a function of R_{ij} to ensure a reliable description of the dependence of the two-center term on R_{ij} in the off-diagonal Hamiltonian matrix element. We found that a representation of $K(R_{ij})$ by

$$K(R_{ij}) = e^{\alpha_K R_{ij}} \quad (12)$$

is quite flexible. The overlap matrix elements $S_{i\alpha,j\beta}(R_{ij})$ are expressed in terms of $S_{ij,\tau}$ with τ denoting, for example, molecular orbitals $ss\sigma$, $sp\sigma$, $pp\sigma$, and $pp\pi$ in a sp^3 configuration. Since they are short-ranged functions of R_{ij} , we chose to represent them by

$$S_{ij,\tau} = (A_\tau + B_\tau R_{ij}) \frac{[1 + e^{-\alpha_\tau d_\tau}]}{[1 + e^{-\alpha_\tau (d_\tau - R_{ij})}]} \quad (13)$$

Based on the orthogonality of the s and p orbitals at the same site, we have

$$A_{ss\sigma} = A_{pp\sigma} = A_{pp\pi} = 1 \quad \text{and} \quad A_{sp\sigma} = 0. \quad (14)$$

Equations (3)–(14) completely define the recipe for constructing semiempirical SCED-LCAO Hamiltonians for materials in terms of parameters and parametrized functions. These parameters, including those characterizing the parametrized functions, are to be optimized with respect to a judiciously chosen database for a particular material.

The total energy of the system consistent with the Hamiltonian described by Eqs. (3)–(14) is given by

$$E_{tot} = E_{BS} - E_{dbc} + E_{ion-ion}, \quad (15)$$

where E_{BS} is the band-structure energy and is obtained by solving the general eigenvalue equation [Eq. (1)], E_{dbc} is the correction to the double counting of the electron-electron interactions between the valence electrons in the band-structure energy calculation, and $E_{ion-ion}$ is the repulsive interaction between ions. Based on Eqs. (3)–(14), Eq. (15) can be rewritten as

$$E_{tot} = E_{BS} + \frac{1}{2} \sum_i (Z_i^2 - N_i^2) U_i - \frac{1}{2} \sum_{i,k(i \neq k)} N_i N_k V_N(R_{ik}) + \frac{1}{2} \sum_{i,k(i \neq k)} Z_i Z_k V_C \quad (16)$$

with

$$V_C = \frac{e^2}{4\pi\varepsilon_0 R_{ik}} = \frac{E_0}{R_{ik}}. \quad (17)$$

It is illuminating to demonstrate how our approach relates to the approach in Ref. 11. We may partition the SCED-LCAO Hamiltonian $H_{i\alpha,j\beta}$ into the two-center term $H_{i\alpha,j\beta}^0$ and the environment-dependent term such that

$$H_{i\alpha,i\alpha} = H_{i\alpha,i\alpha}^0 + (N_i - Z_i)U_i + \sum_{k \neq i} [N_k V_N(R_{ik}) - Z_k V_Z(R_{ik})] \quad (18)$$

and

$$\begin{aligned}
H_{i\alpha,j\beta} = & H_{i\alpha,j\beta}^0 + \frac{1}{2} \left\{ [(N_i - Z_i) + (N_j - Z_j)] U_i \right. \\
& + \left[\sum_{k \neq i} [N_k V_N(R_{ik}) - Z_k V_Z(R_{ik})] \right. \\
& \left. \left. + \sum_{k \neq j} [N_k V_N(R_{jk}) - Z_k V_Z(R_{jk})] \right] \right\} S_{i\alpha,j\beta}(R_{ij}), \quad (19)
\end{aligned}$$

where

$$H_{i\alpha,i\alpha}^0 = \varepsilon_{i\alpha} \quad (20)$$

and

$$H_{i\alpha,j\beta}^0 = \frac{1}{2} K(R_{ij}) (\varepsilon'_{i\alpha} + \varepsilon'_{j\beta}) S_{i\alpha,j\beta}(R_{ij}). \quad (21)$$

Since

$$E_{BS} = \sum_{i\alpha,j\beta} \sum_{\lambda}^{occ} c_{i\alpha}^{\lambda} c_{j\beta}^{\lambda} H_{j\beta,i\alpha} \quad (22)$$

the substitution of Eqs. (18)–(21) to Eq. (22) leads to

$$\begin{aligned}
E_{BS} = & E_{BS}^0 + \sum_i (N_i - Z_i) U_i \left(\sum_{\alpha,\lambda} (c_{i\alpha}^{\lambda})^2 + \sum_{\alpha,j\beta,\lambda} c_{i\alpha}^{\lambda} c_{j\beta}^{\lambda} S_{j\beta,i\alpha} \right) \\
& + \sum_{k \neq i} \sum_i [N_k V_N(R_{ik}) - Z_k V_Z(R_{ik})] \\
& \times \left(\sum_{\alpha,\lambda} (c_{i\alpha}^{\lambda})^2 + \sum_{\alpha,j\beta,\lambda} c_{i\alpha}^{\lambda} c_{j\beta}^{\lambda} S_{j\beta,i\alpha} \right), \quad (23)
\end{aligned}$$

where

$$E_{BS}^0 = \sum_{i\alpha,j\beta} \sum_{\lambda}^{occ} c_{i\alpha}^{\lambda} c_{j\beta}^{\lambda} H_{i\alpha,j\beta}^0 \quad (24)$$

is the band structure energy corresponding to the two-center term. Recognizing that

$$N_i = \sum_{\alpha,\lambda} (c_{i\alpha}^{\lambda})^2 + \sum_{\alpha,j\beta,\lambda(j \neq i)} c_{i\alpha}^{\lambda} c_{j\beta}^{\lambda} S_{j\beta,i\alpha}$$

we obtain

$$\begin{aligned}
E_{BS} = & E_{BS}^0 + \sum_i (N_i - Z_i) N_i U_i \\
& + \sum_{i,k(k \neq i)} [N_k V_N(R_{ik}) - Z_k V_Z(R_{ik})] N_i. \quad (25)
\end{aligned}$$

The substitution of Eq. (25) into Eq. (16) yields

$$\begin{aligned}
E_{tot} = & E_{BS}^0 + \frac{1}{2} \sum_i (N_i - Z_i)^2 U_i + \frac{1}{2} \sum_{i,k(k \neq i)} N_i N_k V_N(R_{ik}) \\
& - \sum_{i,k(k \neq i)} N_i Z_k V_Z(R_{ik}) + \frac{1}{2} \sum_{i,k(k \neq i)} Z_i Z_k V_c(R_{ik}). \quad (26)
\end{aligned}$$

Since

$$V_Z = V_N - \Delta V_N, \quad (27)$$

$$V_C = V_Z + \Delta V_C = V_N - \Delta V_N + \Delta V_C, \quad (28)$$

with

$$\Delta V_C = V_C (1 + B_Z R_{ik}) e^{-\alpha_Z R_{ik}}, \quad (29)$$

the substitution of Eqs. (27) and (28) into Eq. (26) yields

$$\begin{aligned}
E_{tot} = & E_{BS}^0 + \frac{1}{2} \sum_i \Delta N_i^2 U_i + \frac{1}{2} \sum_{i,k(k \neq i)} \Delta N_i \Delta N_k V_N(R_{ik}) \\
& + \sum_{i,k(k \neq i)} N_i Z_k \Delta V_N + \frac{1}{2} \sum_{i,k(k \neq i)} Z_i Z_k (\Delta V_C - \Delta V_N). \quad (30)
\end{aligned}$$

Equation (30) indicates that the total energy in our approach can be expressed as the sum of the two-center band structure energy (first term), Coulomb-like energy associated with the charge fluctuations (second and third terms), and the short-ranged terms (fourth and fifth terms). It reduces to an expression similar to that of Ref. 11 only if we impose the condition $V_N = V_Z$ or $\Delta V_N = 0$, with $E_{rep} = \frac{1}{2} \sum_{i,k(k \neq i)} Z_i Z_k \Delta V_C$. Furthermore, Eq. (30) also shows that, even for systems with no charge redistribution, the total energy expression is different from that of Ref. 11 because of the presence of the term ΔV_N on account of $V_N \neq V_Z$ [E_{SR} = short-range energy = $\frac{1}{2} \sum_{i,k(k \neq i)} Z_i Z_k (\Delta V_C + \Delta V_N)$]. In addition, for such systems, the SCED-LCAO Hamiltonian [see Eqs. (6) and (7)] still contains environment-dependent terms while the Hamiltonian of Ref. 11 no longer has any. The presence of the environment-dependent terms in the Hamiltonian for systems with no on-site charge redistribution affects the distribution of the electrons among the orbitals even though the total charge associated with a given site is not changed. Therefore, the effect of the environment dependency will be reflected in the band structure energy through the solution to the general eigenvalue equation [Eq. (1)] as well as the total energy. This is probably the reason why the results for high-coordinated crystalline phases based on the approach of Ref. 11 do not agree well with the DFT results (see the discussion in Sec. II B).

According to the strategy given above, the framework of the proposed semiempirical SCED-LCAO Hamiltonian will allow the self-consistent determination of the electron distribution at site i . The inclusion of environment-dependent multicenter interactions (three-center explicitly and four-center interactions implicitly) will provide the proposed Hamiltonian with the flexibility of treating the screening effect associated with electrons which is important for the structure stability of narrow band solids such as d -band transition metals, while at the same time, handling the effect of charge redistribution for systems with reduced symmetry on equal footing. Furthermore, as described above, the Hamiltonian is set up in such a way that the physics underlying each term in the Hamiltonian is transparent. Therefore, it will be convenient to trace the underlying physics for properties of a system under consideration when such a Hamiltonian is used to investigate a many-atom aggregate and predict its properties. The salient feature of our strategy is that, with the incorporation of all the relevant terms discussed previously,

TABLE I. Parameters of the SCED-LCAO Hamiltonian for silicon.

Symbols	Values	Symbols	Values	Symbols	Values
U	8.05 eV	α_N	2.74 Å ⁻¹	$\alpha_{sp\sigma}$	2.18 Å ⁻¹
ε'_s	-13.43 eV	d_N	1.91 Å	$\alpha_{pp\sigma}$	2.35 Å ⁻¹
ε'_p	-7.91 eV	$B_{ss\sigma}$	0.88 Å ⁻¹	$\alpha_{pp\pi}$	3.74 Å ⁻¹
α_K	0.25 Å ⁻¹	$B_{sp\sigma}$	-0.75 Å ⁻¹	$d_{ss\sigma}$	1.32 Å
B_Z	1.54 Å ⁻¹	$B_{pp\sigma}$	-0.79 Å ⁻¹	$d_{sp\sigma}$	1.35 Å
A_N	-1.26 eV	$B_{pp\pi}$	-0.31 Å ⁻¹	$d_{pp\sigma}$	2.03 Å
B_N	0.16 eV Å ⁻¹	$\alpha_{ss\sigma}$	3.04 Å ⁻¹	$d_{pp\pi}$	2.28 Å

there is no intrinsic bias towards ionic, covalent, or metallic bonding for the proposed Hamiltonian. Thus our strategy represents an approach that provides the appropriate conceptual framework to allow the chemical trend in a given atomic aggregate to determine the structural as well as electronic properties of condensed matter systems. In our strategy, there will be only about 20 fitting parameters in the construction of the proposed Hamiltonian for single component systems with a sp^3 basis. Our approach requires far less parameters compared to phenomenological approaches^{3,4} (with ~ 50 to 100 parameters) where environment-dependent effects are emphasized. In addition, the roles played by these parameters are well defined in terms of their physical significance. With far fewer parameters needed for the description of the proposed Hamiltonian, the optimization scheme for the determination of these parameters will be more robust. In our strategy, these parameters will be fitted to properties of stable configurations obtained from experiments and/or reliable first principles calculations, as well as metastable configurations determined by first principles calculations. Our approach differs from the DFT-based TB approach of Ref. 11 in the following important aspects. (1) A uniform treatment of the environment-dependent multicenter interactions for systems with or without the charge redistribution, resulting in a transferable Hamiltonian for a wide range of phases for materials beyond the scope of the approach in Ref. 11 as well as all other existing approaches. It should be noted that our treating environment-dependent interactions for systems with or without the charge redistribution on an equal footing highlights the important feature, the difference between $V_N(R_{ik})$ and $V_Z(R_{ik})$, that plays the crucial role in modeling the effects of electron screening in an atomic aggregate and that is completely ignored in the approach of Ref. 11. (2) A database-driven semiempirical approach. Our approach depends critically on the database. If one can judiciously compile a systematic and reliable database, our scheme has the flexibility to allow the database to properly model the screening effect of the electrons in an atomic aggregate.

We have also implemented a MD scheme based on the SCED-LCAO Hamiltonian. In the MD simulations, the forces acting on the atoms in the atomic aggregate must be calculated at each MD step. The calculation of the band structure contribution to atomic forces can be carried out by the Hellmann-Feynman theory.¹⁴ With the presence of terms involving N_i and N_k in the SCED-LCAO Hamiltonian [see

TABLE II. Comparisons of bond lengths (Å) and binding energies (eV) for different geometries of Si clusters obtained using the SCED-LCAO method and *ab initio* calculations (Ref. 17).

Cluster	Symmetry	Present work	<i>ab initio</i> values
Si ₂	D_{ih}	2.226 Å	2.288 Å
		-2.435 eV	-2.499
Si ₃	C_{2v}	2.284 Å	2.357 Å
		2.168 Å	2.158 Å
Si ₃	D_{ih}	-3.413 eV	-3.575 eV
		2.141 Å	2.167 Å
Si ₃	D_{ih}	-3.427 eV	-3.404 eV
		2.275 Å	2.311 Å
Si ₄	D_{2h}	-4.101 eV	-4.242 eV
		2.332 Å	2.474 Å
Si ₄	T_d	-3.773 eV	-3.659 eV
		2.116 Å	2.156 Å
Si ₄	D_{1h}	2.164 Å	2.176 Å
		-3.289 eV	-3.364 eV
Si ₅	D_{3h}	2.207 Å	2.306 Å
		3.141 Å	3.064 Å
Si ₅	C_{4v}	-3.352 eV	-3.340 eV
		2.209 Å	2.275 Å
Si ₅	C_{4v}	2.358 Å	2.513 Å
		-4.327 eV	-4.266 eV
Si ₅	D_{ih}	2.082 Å	2.133 Å
		2.128 Å	2.144 Å
Si ₅	D_{ih}	-3.545 eV	-3.534 eV
		2.127 Å	2.215 Å
Si ₅	T_d	3.475 Å	3.617 Å
		-3.334 eV	-3.383 eV
Si ₆	D_{4h}	2.248 Å	2.363 Å
		2.639 Å	2.734 Å
Si ₆	D_{4h}	-4.698 eV	-4.664 eV
		2.261 Å	2.285 Å
Si ₆	D_{3d}	2.948 Å	3.208 Å
		-3.896 eV	-3.972 eV
Si ₆	D_{3d}	2.057 Å	2.098 Å
		2.072 Å	2.134 Å
Si ₆	D_{ih}	2.149 Å	2.158 Å
		-3.446 eV	-3.446 eV

Eqs. (5)–(7)], terms such as $\nabla_k N_i$ where ∇_k refers to the gradient with respect to \vec{R}_k will appear in the electronic contribution to the atomic forces. However, these terms are canceled exactly by terms arising from the gradients of the second and the third terms in the total energy expression [Eq. (16)]. Thus terms involving $\nabla_k N_i$ will not contribute to the calculation of atomic forces. This fact greatly simplifies the calculation of atomic forces needed in the MD simulations. In other words, if one disregards the extra time due to the self-consistency requirement, the calculation of atomic forces based on the SCED-LCAO Hamiltonian is not any-

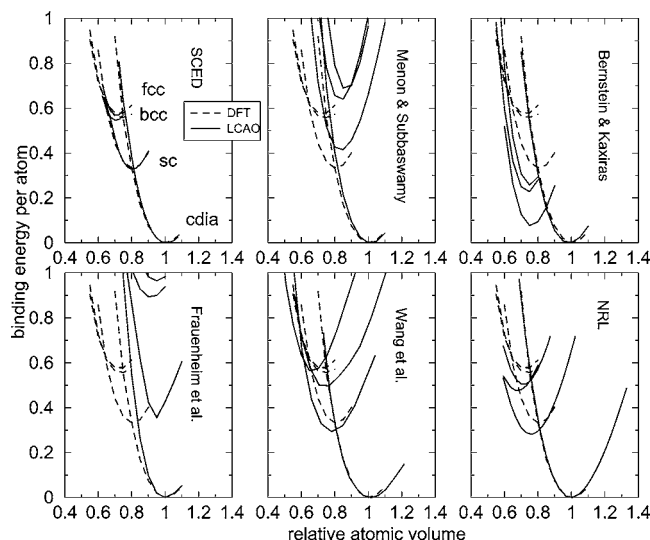


FIG. 1. The binding energy vs relative atomic volume curves for the diamond (cdia), the simple cubic (sc), the body centered cubic (bcc), and the face centered cubic (fcc) phases of silicon, obtained using the present SCED-LCAO scheme (top-left panel). The corresponding curves obtained using three existing traditional (two-center and non-selfconsistent) nonorthogonal tight binding (NOTB) Hamiltonians [top-central (Ref. 23), top-right (Ref. 24), and bottom-left (Ref. 22) panels] and two more recently developed non-selfconsistent but environment-dependent Hamiltonians bottom-central (Ref. 9) and bottom-right (Ref. 7) panels] are also shown in the figure. All the curves (solid) are compared with the result obtained by a DFT-LDA calculation (Ref. 18) (dotted).

more difficult compared with conventional TB approaches.

Finally, when there is charge redistribution, the Ewald's method¹⁵ can be used to calculate the long-range Coulomb interactions for extended systems. For finite systems, direct summation of the Coulomb terms can be used.

B. Optimized parameters and results for bulk silicon

The parameters characterizing our SCED-LCAO Hamiltonian are determined by an efficient global optimization procedure against an appropriately chosen database, by adapting a local least-squares algorithm, the Marquardt-Levenberg algorithm,¹⁶ to the global problem. A brief description of this procedure is described in Appendix A. For single-component systems with sp^3 basis, there are about 20 parameters defining the SCED-LCAO Hamiltonian. The parameters characterizing the SCED-LCAO Hamiltonian for silicon, obtained using the optimization procedure outlined in Appendix A, are given in Table I. The properties used to determine this set of parameters include: (i) the binding energies and bond lengths for Si_n clusters with $n=2$ to 6 (shown in Table II),¹⁷ (ii) the binding energy vs atomic volume curves for the diamond, the simple cubic (sc), the body centered cubic (bcc), and the face centered cubic (fcc) phases,¹⁸ respectively (shown in Fig. 1), and (iii) the band structure energies at high symmetry points for the diamond phase¹⁸⁻²¹ (shown in Fig. 2 and Table III).

The results showing the binding energy vs relative atomic volume curves for the diamond, the simple cubic (sc), the

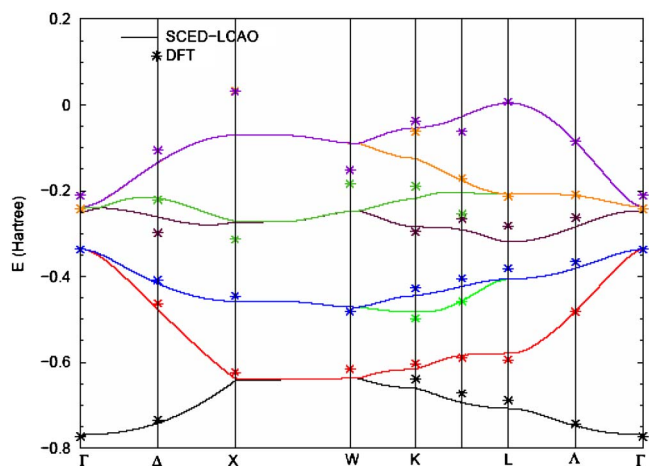


FIG. 2. (Color online) The band structure of bulk Si calculated for the diamond phase using the SCED-LCAO approach and the corresponding DFT band structure (stars) taken from Ref. 18 are shown.

body centered cubic (bcc), and the face centered cubic (fcc) phases of silicon, obtained by using the SCED-LCAO Hamiltonian constructed for Si with our scheme, are presented in Fig. 1. Also shown in Fig. 1 are the corresponding curves obtained using three existing traditional (two-center and non-selfconsistent) nonorthogonal tight binding (NOTB) Hamiltonians,²²⁻²⁴ and two more recently developed non-selfconsistent but environment dependent Hamiltonians.^{7,9} All the curves (solid) are compared with the results obtained by DFT-LDA calculations¹⁸ (dotted). It can be seen that while the results obtained by all the existing Hamiltonians fail for the high-pressure phases, those obtained using Hamiltonians with environment-dependent terms give much better agreement for those phases. This is an indication of the importance of the inclusion of the environment dependent effects in the Hamiltonian, even for single-element extended crystalline phases. However, the most striking message conveyed by Fig. 1 is how well our result compares with the DFT-LDA results for all the extended crystalline phases, both at low as well as high pressures. It indicates that our scheme

TABLE III. Band structure energies (in eV) at high symmetry points of bulk Si obtained from the present work (optimized lattice constant is 5.4464 Å) are compared with the DFT calculation and experimental results.

Band index	Present work	DFT calculation	Experiment
Γ_{1v}	-11.77	-11.93 ^a	-12.4±0.6; ^b -12.5±0.6 ^c
X_{4v}	-3.30	-2.88 ^a	-2.5±0.3; ^c -2.9 ^d
$L_{2'v}$	-10.10	-9.52 ^a	-9.3±0.4 ^c
L_{1v}	-6.62	-7.00 ^a	-6.4±0.4; ^b -6.8±0.2 ^c
L_{3v}	-1.89	-1.20 ^a	-1.2±0.2 ^d

^aReference 18.

^bReference 19.

^cReference 20.

^dReference 21.

TABLE IV. The equilibrium lattice constant, the cohesive energy per atom, the bulk modulus, and the elastic constants of silicon in the diamond phase as obtained using the SCED-LCAO method (second column) are compared with the corresponding results as obtained by other semiempirical approaches (third column), DFT-based methods (fourth column), and experiments (fifth column).

Properties	SCED-LCAO	Other TB	DFT	Expt.
Lattice constant (Å)	5.443	5.426; ^e 5.399; ^f 5.427; ^g 5.417 ^h	5.451; ^a 5.399 ^f	5.429 ^b
Cohesive energy (eV/atom)	4.904	4.71; ^f 5.19; ^g 4.97 ^h	4.67; ^a 4.70 ^f	4.63 ^c
Bulk modulus (GPa)	96.6	108.3; ^e 104.8; ^f 153.5; ^g 115.1 ^h	98; ^a 96.4; ^e 98 ^f	99 ^d
C11 (GPa)	166.3	179; ^e 145; ^f 218; ^g 185 ^h	152 ^e	166 ^d
C12 (GPa)	61.7	73; ^e 84.5; ^f 121; ^g 80.1 ^h	60 ^e	64 ^d
C44 (GPa)	93.7	95 ^e	101 ^e	80 ^d

^aReference 18.

^bThe experimental zero-pressure lattice constants and atomic volumes at 0 K are obtained from J. Donohue, *The Structure of Elements* (Wiley, New York, 1974), corrected for thermal expansion and atmospheric-pressure compression.

^cL. Brewer, Lawrence Berkeley Laboratory Report No. LBL-3720 (unpublished) (for the cohesive energy at 0 K); C. E. Moore, *Atomic Energy Levels* [National Bureau of Standards, Washington, D.C., 1949 (Circular No. 467, Vol. 1)].

^dH. J. McSkimin, *J. Appl. Phys.* **24**, 988 (1953); H. J. McSkimin and P. Andreatch, Jr., *ibid.* **34**, 651 (1963); *ibid.* **35**, 2161 (1964). The elastic moduli were measured at 77 K.

^eReference 7.

^fReference 24.

^gReference 23.

^hReference 22.

has the capacity and the flexibility of capturing the environment-dependent screening effect under various local configurations.

To further demonstrate the reliability of the SCED-LCAO Hamiltonian for predicting system properties, we have calculated the band structure of bulk Si in the diamond phase in all directions. The result and its comparison with the available DFT-based calculation¹⁸ are shown in Fig. 2. It can be seen that the agreement between these two sets of results is excellent in terms of both the trend and the magnitude for the valence band, although the agreement is not as good for the conduction band. We have also calculated the elastic constants of the diamond phase. Since the calculation of elastic constants involves the second derivatives of the energy at its minimum corresponding to the equilibrium configuration, the result is extremely sensitive to the accuracy of the semiempirical Hamiltonian used in the calculation. Hence the calculation of elastic constants provides a stringent test for the reliability of the SCED-LCAO Hamiltonian. In Table IV, the results of our calculations of bulk modulus and elastic constants are shown, together with the corresponding results obtained by other semiempirical Hamiltonians, DFT-based methods, and experimental measurements. It can be seen that our results agree very well with the experimental measurements and DFT results. This agreement is far better than those that were achieved by other existing semiempirical calculations. In fact, our agreement with the experimental measurements is as good as that achieved by DFT-based calculations. This comparison shows definitively the reliability of the SCED-LCAO Hamiltonian constructed for Si. We have also checked the self-consistency in the charge redistribution

by using the SCED-LCAO Hamiltonian to study the structural properties of Si_n clusters with *n* ranging from 2 to 6. The results on the binding energy and bond lengths for the stable and metastable structures of these clusters all agree excellently with the first principles results¹⁷ (see Table II).

III. APPLICATIONS

In this section, the robustness of the SCED-LCAO Hamiltonian is elucidated through several examples. We demonstrate that the parameters of SCED-LCAO Hamiltonian obtained by fitting them to the bulk silicon and small silicon clusters (atoms up to 6) are capable of predicting the structural properties of intermediate size silicon clusters and complex silicon surfaces. Specific examples studied include: (A) structural properties of Si₇₁ cluster, (B) reconstruction of the Si(001) surface, and (C) the energy landscape of a Si monomer adsorbed on the reconstructed Si(111)-(7×7) surface.

A. Structural properties of Si₇₁ cluster

We have used the MD scheme based on the SCED-LCAO Hamiltonian to determine the stable structure of Si₇₁, an intermediate-size cluster. We generated the initial configuration of Si₇₁ cluster from the truncated tetrahedral network. We first heated and equilibrated this initial configuration at 500 K for about 2.4 ps. We then annealed it to 300 K for about 0.7 ps, and finally cooled it down to 0 K for about 2 ps.

The atoms on the truncated “surface” of the initial tetrahedral configuration of the Si₇₁ cluster have many dangling

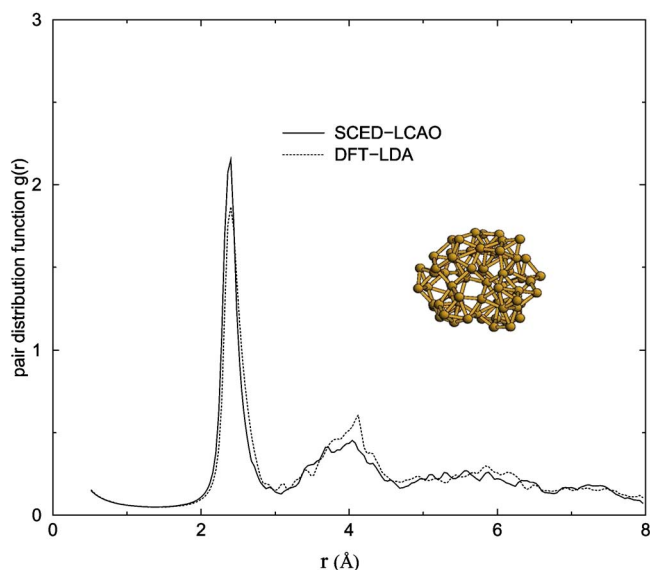


FIG. 3. (Color online) The pair-distribution function $g(r)$ for the relaxed Si_{71} cluster (inset) calculated from the SCED-LCAO method (solid) is compared with the DFT-LDA calculation (Ref. 29) (dotted).

bonds. Therefore the initial configuration is very unstable. Two factors that play key roles in determining a stable configuration of a Si cluster are: (1) saturation of the dangling bonds of the surface atoms; (2) the tendency to maintain the coordination number for Si atoms closer to four. The interplay of these factors will lead to a distorted surface for a stable Si cluster. This can be seen from the inset of Fig. 3 where the stabilized Si_{71} cluster obtained by our simulation shows a compact network in a more oblate structure. The strong surface distortion is a reflection of local bonding configurations with the number of bonds associated with atoms in the cluster, in particular the surface atoms, close to four.

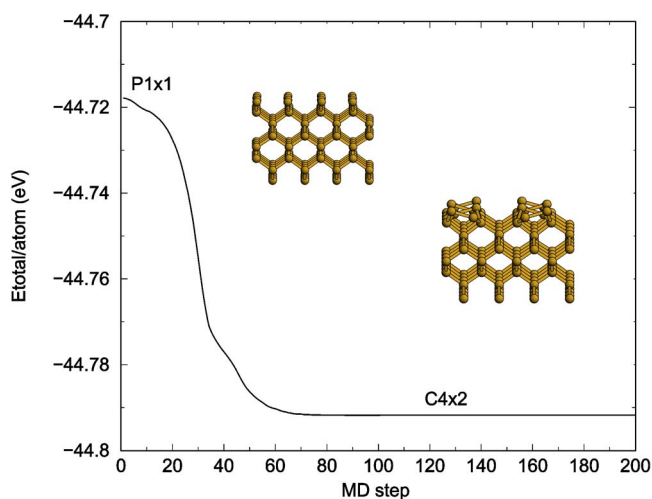


FIG. 4. (Color online) Total energy calculations as a function of MD steps (1 step=2.5 fs) in the SCED-LCAO MD simulation reveal the $C4 \times 2$ reconstruction (right inset) as the most stable structure for the Si (100) surface with ideal $P1 \times 1$ symmetry (left inset) as the initial configuration.

TABLE V. Characteristics of the buckled dimer row on the $\text{Si}(001)$ $C4 \times 2$ reconstructed surface: $\Delta E/\text{dimer}$ is the binding energy per dimer (in eV), b denotes the dimer bond length (in Å), Δz the height of the bulked dimer (in Å), and α the angle of the dimer with respect to the surface (in degree).

Properties	Present work	DFT-LDA	Experiment
$\Delta E/\text{dimer}$	1.18	1.39 ^a	
b	2.47	2.29 ^a	2.45 ± 0.1^b
Δz	0.69	0.69 ^a	
α	16.19	17.5 ^a	

^aReference 30.

^bReference 31.

This type of structure has also been found to be more stable for other Si clusters of intermediate size by previous theoretical studies.^{25–28}

We have also calculated the pair distribution function $g(r)$ for the equilibrated Si_{71} cluster (see the inset of Fig. 3). From Fig. 3, it can be seen that $g(r)$ exhibits a very sharp first peak followed by a broader second peak, a typical feature of distorted cluster structure. Also shown in Fig. 3 is the pair distribution function for the stable Si_{71} cluster obtained under the same equilibration procedure but using the DFT-based fire-ball MD scheme.²⁹ It can be seen that the agreement between the result from the SCED-LCAO MD scheme and that from the fire-ball MD scheme is excellent.

It is well known that the charge redistribution plays the critical role in establishing chemical bonding in relaxation. This is particularly true for surface atoms in a cluster of intermediate size. The result of our test case therefore has demonstrated the robustness of the self-consistent scheme in the determination of the charge redistribution in the SCED-LCAO Hamiltonian.

B. Reconstruction of the $\text{Si}(001)$ surface

We have carried out a MD simulation of the reconstruction of $\text{Si}(001)$ surface from scratch, using the SCED-LCAO Hamiltonian. We started with the ideal $\text{Si}(001)$ with $P1 \times 1$ symmetry as the initial configuration. We chose a 4×4 slab with a thickness of eight layers as the MD cell. In the simulation, the atoms in the top four layers were allowed to fully relax while the atoms in the bottom four layers were kept at their bulk equilibrium positions. We turned on the simulations by first moving the surface atoms in the alternate column towards the fixed surface atoms by ≤ 0.1 Å (see the left inset of Fig. 4).

We found that the surface reconstruction of the $\text{Si}(001)$ surface using SCED-LCAO takes about 0.5 ps (see Fig. 4). The surface atoms begin to dimerize in ~ 0.05 ps after performing the SCED-LCAO MD relaxation. These dimers become buckled (tilted) after about another 0.075 ps. Finally the surface reconstruction stabilizes to the stable configuration with the $C4 \times 2$ symmetry (see the right inset of Fig. 4) in another ~ 0.375 ps. To the best of our knowledge, this is the first time that the $C4 \times 2$ reconstruction of the $\text{Si}(001)$ surface is obtained directly from the dynamical relaxation

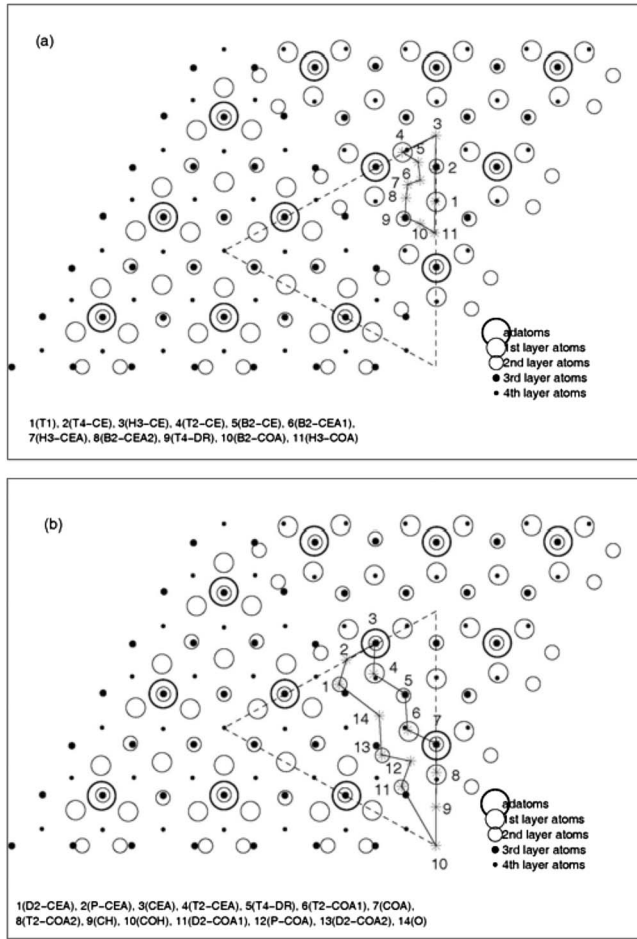


FIG. 5. Shown are sites (denoted as stars) in the irreducible region (bounded by the dashed triangle) along which the adsorption energies of a monomer on Si(111) 7×7 reconstructed surface are calculated. The sites along the first pathway (a) and the second pathway (b) lie in the faulted half. The footnote shows the correspondence between site numbers and symbols.

simulation of its ideal $P1 \times 1$ surface configuration. It demonstrates the predictive power of the SCED-LCAO Hamiltonian. We also found that the $C4 \times 2$ configuration can not be obtained when the simulation is performed without the self-consistent requirement of the charge, indicating that charge redistribution is a key ingredient during the surface reconstruction.

In Table V, the properties characterizing the buckled $C4 \times 2$ reconstruction of the Si(001) surface obtained by the SCED-LCAO Hamiltonian-based MD simulation are compared with the corresponding properties obtained by DFT calculation³⁰⁻³² and/or experimental measurements.³³ It can be seen that the agreement is very good.

C. Mapping the energy landscape of a Si monomer adsorbed on the reconstructed Si(111)-(7 \times 7) surface

Finally, we have applied the SCED-LCAO Hamiltonian to map out the energy landscape for a Si monomer adsorbed on the reconstructed Si(111) surface.³⁴ This represents a most stringent test for the reliability and efficiency of the applica-

tion of the SCED-LCAO Hamiltonian because of the complicated reconstruction of the Si(111) surface. In our study, we used the SCED-LCAO-MD scheme to unravel the structural and the dynamical behavior of an adsorbed Si atom on the Si(111)-(7 \times 7) dimer-atom-stacking-fault (DAS)-reconstructed surface.³⁵ To have a complete understanding of the behavior pattern of the Si adsorbate on the Si(111)-7 \times 7 surface, we first confirmed, using SCED-LCAO-MD, that the SCED-LCAO Hamiltonian for Si can indeed lead to the reconstructed 7 \times 7 DAS structure, including both the faulted and the unfaulted halves. In this case, by necessity, we have used a large supercell composed of 10 layers plus the adatom layer (494 atoms in total), where the top eight layers were relaxed and the bottom two layers were held at their bulk equilibrium positions.

We determined the preferential adsorption sites for an adsorbed Si atom by mapping out the total energy as a function of its positions on the surface. In Figs. 5(a) and 5(b) the adsorption energy along two pathways in the faulted half of the unit cell is shown, respectively. These two pathways are composed of irreducible sites in the faulted half. The site symbols are described as follows: *T1* denotes an adsorption site on top of the rest atom with one dangling bond, *T2* a site on top of layer-1 atom which is different from the rest atom, *T4* a fourfold site on top of an undimerized atom of layer-2, *H3* a hexagonal threefold site, *B2* a twofold site between *T4* and *H3* or *T2* and *T4*, *D2* a site on top of a dimer atom, *P* a site within the pentagonal ring and whose image site in the unfaulted half lies above a layer-4 atom, *O* a site within an octagonal ring and whose image site in the unfaulted half lies above a layer-4 atom, *CH* a site within the corner hole region and whose image site in the unfaulted half lies above a layer-4 atom, *CEA* a site on top of a central adatom, *COA* a site on top of a corner adatom, and *COH* the central position of the corner hole, respectively. In addition, the auxiliary notation *CE* denotes a site located in the central region of the half unit cell, *CEA* a site located near the central adatom, *COA* a site located near the corner adatom, and *DR* a site located near the dimer row, respectively. As shown in Table VI, the calculated adsorption energies for sites along the two pathways in the faulted half exhibit many stable adsorption sites (*T4-CE*, *T2-CE*, *B2-CEA1*, *B2-CEA2*, *B2-COA*, and *H3-COA* along the path 1 and *T2-CEA*, *T4-DR*, *T2-COA1*, *T2-COA2*, *O*, and *CH* along the path 2). It is interesting to note that the stable adsorbate site is not on top of the rest atom (*T1*) or on top of the dimers (*D2*). The factor determining the stable adsorbate sites depends on the situation when, in addition to saturating any dangling bond of the surface atoms, the Si adsorbate atom can form more bonds with the substrate atoms so that its coordination number is closer to four. The adsorbed Si atom at site *T1*, although it saturates one dangling bond of the rest atom, does not satisfy the optimally coordinated criterion for silicon. Our calculation also reveals several low-energy barriers in both pathways, in particular, energy barriers of ≤ 0.3 eV between the sites *T2-CE* and *B2-CEA1*, *B2-CEA1* and *B2-CEA2*, or *B2-CEA2* and *B2-COA*, or two equivalent *B2-COAs* in pathway 1 and between the sites *T2-COA1* and *T2-COA2*, or between two equivalent *T2-CEA* sites in the pathway 2. These results are consistent with the result of theoretical calculations using the DFT-based VASP package.³⁶

TABLE VI. Calculated adsorption energies for a Si monomer adsorbed in the irreducible region of Si(111)-(7×7) reconstructed surface.

Site number along path 1	$E_{\text{adsorption}}$ (eV) (faulted)	$E_{\text{adsorption}}$ (eV) (unfaulted)	Symbol of the site type
1	-3.12048	-3.29868	T1
2	-4.15503	-4.00158	T4-CE
3	-3.55113	-3.35263	H3-CE
4	-3.91248	-3.90753	T2-CE
5	-3.64064	-3.47482	B2-CE
6	-3.97138	-4.06098	B2-CEA1
7	-3.70458	-3.49668	H3-CEA
8	-3.95703	-3.97188	B2-CEA2
9	-3.77883	-3.88883	T4-DR
10	-4.22929	-4.11543	B2-COA
11	-3.94705	-3.37095	H3-COA

Site number along path 2	$E_{\text{adsorption}}$ (eV) (faulted)	$E_{\text{adsorption}}$ (eV) (unfaulted)	Symbol of the site type
1	-3.04120		D2-CEA
2	-3.52638	-3.37293	P-CEA
3	-2.67844	-2.68537	CEA
4	-3.76398	-3.78279	T2-CEA
5	-3.77883	-3.77883	T4-DR
6	-4.08573	-4.03078	T2-COA1
7	-2.97190	-3.01653	COA
8	-3.88773	-3.81348	T2-COA2
9	-3.85308	-3.44718	CH
10	-2.93238		COH
11	-3.33332		D2-COA1
12	-3.53133	-3.75408	P-COA
13	-3.20463		D2-COA2
14	-3.83320	-3.14028	O

Based on the energy landscape, the low barrier energies, and the fact that the sites are located close to each other, one can expect the adsorbed Si atom to be trapped in one of the three types of basins of attraction in the faulted half described as follows (see Fig. 6).

(1) Triangular-type basin: The energy landscape calculation reveals three triangular-type basins of attraction surrounding the T1 sites on top of the rest atom, formed by sites of B2, H3, and T4 type as shown in Fig. 6. In each of the basins of attraction, the adsorption energy near the corner adatoms (i.e., the B2-COA and H3-COA sites) is lower than that near the central adatoms (i.e., the B2-CEA and H3-CEA sites). This anisotropy in energy in the triangular type of basin is consistent with the atom tracking image of an adsorbed Si atom at low temperatures [see Fig. 4(a) of Ref. 37], where it is reported that the adsorbed atom spends most of the time in the region defined by the positions R1, R2, R3 which are near the rest atoms and the corner adatoms COA1, COA2, and COA3.

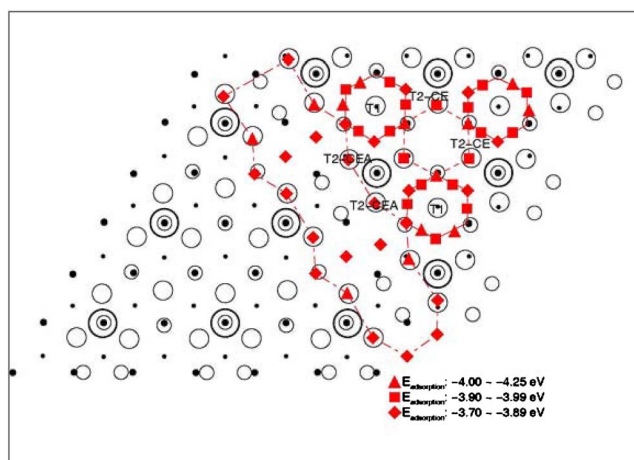


FIG. 6. (Color online) Three basins of attractions (triangular-type, hexagonal ring-type, and shoulder-type, respectively) for a silicon monomer on the Si(111)-7×7 reconstructed surface are shown, with the triangle, the square, and the diamond indicating the energies in increasing order. The sites denoted by T1, T2-CE, and T2-CEA, which are bounded by the three basins of attraction, confirms the existence of the experimentally observed region of six protrusions associated with the magic clusters (Ref. 39).

(2) Hexagonal ring-type basin: As shown in Fig. 6, a hexagonal ring-type basin of attraction is located at the center of the half unit cell and is composed of the T2-CE and T4-CE sites surrounding the H3-CE site with the T4-CE site having the lowest energy. This type of the basin of attraction provides the explanation for the atom-tracking image of an adsorbed Si atom at room temperature,³⁷ where it is reported that the adsorbed atom spends most of the time inside the central region defined by the three center adatoms (CEA1, CEA2, and CEA3), but occasionally moves near the rest atom positions (R1, R2, or R3) and corner adatom (COA1 or COA2) positions, as shown in Fig. 2(a) of Ref. 37.

(3) Shoulder-type basin: The energy landscape calculated along pathway-2 reveals shoulder-type basin of attraction in the vicinity of the dimer row formed by the O, T2-CEA, T4-DR, T2-COA1, T2-COA2, and CH sites, as shown in Fig. 6. The T2-COA sites near the corner holes are lower in energy. This may explain the formation of the Si tetramers located on the top of the corner dimer at low temperature and on the top of central dimer at room temperature.^{37,38}

The combination of the three types of basins of attraction results in an attractive potential well that traps the adsorbed Si atoms to form magic clusters. In particular, the region bounded by T2-CE, T2-CE, T1, T2-CEA, T2-CEA, and T1 (as shown in Fig. 6) matches very well the schematic drawing of the six protrusions depicting the magic cluster on the faulted half of Si(111)-7×7 surface as noted by Hwang *et al.*³⁹ Furthermore, the low energy barriers allow the cluster to move within the half unit cell.

We have also compared adsorption energies of corresponding sites in the faulted half and the unfaulted half of the unit cell. We found that the adsorption energy of most of the sites in the faulted half is lower compared with the corresponding site in the unfaulted half (see Table VI). Specifically, the sites with the two lowest energy, B2-COA and

TABLE VII. Computational speeds and memory usages in the relaxation of a Si_{71} cluster are compared for the SCED-LCAO and VASP (Γ point, $E_{\text{cut}}=150$ eV, $25 \times 25 \times 25$ super cell) methods. The number of self-consistent loops for the initial MD step (1), an intermediate step (30), and for full relaxation are also shown. This calculation was done on a single 1.6-GHz AMD Athlon MP processor.

Method	MD steps	Number of self-consistent loops per MD	Wall time	Memory
VASP	1	25	~3 h 9 m	~300 MB
	30	average 17	~18 h	
	191-fully relaxed	average 9	~189 h 22 m 33 s	
SCED-LCAO	1	15	~34 m	~63.4 MB
	30	average 17	~34 m	
	600-fully relaxed	average 4	~6 h 55 m	

T4-CE, have lower energy in the faulted half than in the unfaulted half. This appears to be one of the reasons why the Si magic cluster prefers to form on the faulted half of the unit cell of $\text{Si}(111)-(7 \times 7)$ surface as observed by Hwang *et al.*³⁹

IV. CONCLUDING REMARKS AND FUTURE OUTLOOK

The application of the SCED-LCAO Hamiltonian for silicon to the three test cases discussed above represents a concerted effort to test the versatility, the reliability, and the efficiency of using the SCED-LCAO Hamiltonian to study properties of complex systems with no or reduced symmetry. The first case concerns a finite system with no symmetry. The second and third cases deal with extended systems with reduced symmetry. The properties of all these three low-dimensional systems are, therefore, critically dependent on charge redistribution and environment-dependent multicenter interactions. The result of our test studies has clearly demonstrated that (i) the SCED-LCAO Hamiltonian for silicon is transferable and hence it has the predictive power; (ii) the self-consistent scheme for the determination of the charge redistribution is robust; (iii) the MD code based on the SCED-LCAO Hamiltonian is efficient.

A comparison of computational speed and memory usage of the SCED-LCAO with the DFT-based Vienna *ab initio* simulation package (VASP) reveal that the SCED-LCAO is about 30 times faster than the VASP calculation and it requires about five times less memory for the relaxation of a Si_{71} cluster (see Table VII). In addition, by implementing the order- N scheme into the framework of the SCED-LCAO Hamiltonian for total energy and force calculations, we found that we can perform full geometry optimization of systems of sizes about 20 000 atoms.⁴⁰ Thus reliable large-scale quantum-mechanics based MD simulations are attainable using the $O(N)$ /SCED-LCAO scheme. The size limita-

tion in our scheme arises mainly from the bottleneck associated with the Ewald summations.

In a forthcoming publication, the SCED-LCAO Hamiltonian will be used to study the relative stability of 1D Si nanowires (NWs) of different orientations with diameters ranging from a few to 15 nm. The study of larger diameter SiNWs requires the implementation of the $O(N)$ algorithm into the SCED-LCAO approach and a parallelized version of the SCED-LCAO/MD code.

The development of a recipe to construct semiempirical Hamiltonians for elemental materials in the present work is grounded in the ingredients of the many-body Hamiltonians describing the many-atom aggregates.⁴¹ The determination of the parameters characterizing the SCED-LCAO Hamiltonians is database driven. In this sense, the SCED-LCAO Hamiltonian is only as good as the database used to optimize the fitting parameters. Our case studies on silicon-based structures indicate that, with the compilation of a judiciously chosen database, the resulting SCED-LCAO Hamiltonian is versatile, reliable, efficient, and possesses predictive power. Thus, we are confident that reliable and transferable SCED-LCAO Hamiltonians with predictive power can be developed for real materials using our scheme. Furthermore, our scheme is efficient so that simulations of complex systems with large degrees of freedom can be conveniently carried out.

Construction of SCED-LCAO Hamiltonians for other column IV elements (e.g., carbon and germanium), simple metals (e.g., aluminum), and transition metals (e.g., iron and nickel) are currently in progress with very encouraging results. For example, the stable structure of bucky diamond (C_{147}) (Ref. 42) was predicted using our preliminary SCED-LCAO Hamiltonian for C while it cannot be correctly predicted by other semiempirical approaches. The extension of the present scheme to its spin-polarized version and to heterogeneous systems is also in progress.

ACKNOWLEDGMENTS

We would like to acknowledge helpful discussions with Weitao Yang. This work was supported by the NSF (Contract No. DMR 0112824) and the U.S. DOE (Contract No. DE-FG02-00ER45832).

APPENDIX: AN OUTLINE OF THE OPTIMIZATION SCHEME

The first step in the optimization procedure is to define a *residual* or *objective function* R which depends on the parameters s_i of the SCED-LCAO Hamiltonian, and for which the minimum value of R is interpreted as the best value. We use a least-squares sum of the differences between the calculated properties P_{calc} and the reference values P_{ref}

$$R(s_i) = \sqrt{\frac{1}{N_p} \sum_k \left(P_{\text{weight}}^k \frac{P_{\text{calc}}^k - P_{\text{ref}}^k}{P_{\text{scale}}^k} \right)^2}. \quad (\text{A1})$$

This expression also includes the characteristic scale P_{scale} of each property, a weight factor P_{weight} which represents the

relative importance of each property, and the total number of properties N_p . The use of the scale, weight, and number of properties allows for the interpretation of the residual as the average relative deviation of the calculated values from the reference values.

The optimization problem is to find the *global* minimum, which is the set s_i which has the absolute smallest value of R . Optimization algorithms, however, are fundamentally related to the number and distribution of *local* minima. In the easiest case, there would be only one local minimum, and only about 10^3 evaluations of R would be needed to find the global minimum. In the worst case, the local minima would be distributed randomly, and only a brute force search could find the global minimum. In this worst case scenario, the number of function evaluations needed would be $G_s^{N_s}$, where G_s is the number of points for each parameter, and N_s is the number of parameters. A reasonable value of G_s is ~ 200 , and with ~ 20 semiempirical parameters it is evident that the optimization problem would be intractable. This means that the selection of the optimization algorithm, and also the selection of the initial or starting values of the semiempirical parameters, is particularly important.

For the initial inputs in parameter-fitting, we use results adapted from the available literature. For example, first-principles calculations of the overlap matrices such as $S_{ss\sigma}$ are available for Si.²² For the least squares problem with N_p on the order of 10^2 , there are of the order of 10^2 terms in the summation. If this summation is performed explicitly, a large amount of information about the individual behavior of these terms is lost. For example, if the summation is performed explicitly, the only information available about the derivatives is the gradient $\frac{\partial R}{\partial s_i}$ with N_s elements, but if the summation is not performed explicitly then the entire Jacobian $\frac{\partial P^k}{\partial s_i}$ with $N_s N_p$ elements is available. So even though the problem is to find the minimum value of R , efficient least-squares algorithms do not perform the summation explicitly, but rather store and analyze each of the 10^2 terms in the summation. This is the approach used by the Marquardt-Levenberg algorithm,¹⁶ which is a widely used and highly efficient algorithm for finding the local minimum of a least-squares problem. When compared with any algorithm which analyzes only the value of R , least-squares algorithms are typically one or two orders of magnitude more efficient at finding the local minimum, with the efficiency increasing for larger values of N_p .

Now, the least-squares problem and the Marquardt-Levenberg algorithm are well understood.¹⁶ Also, the global optimization problem for a scalar function is well understood.¹⁶ However, we have here a *global least-squares* problem. There are two general approaches to the global least-squares problem. The first is to treat the least-squares problem as a scalar optimization problem, analyzing only the value of R and not the values of the individual least-squares terms. The reasoning here is that the benefit of using pre-existing and well-understood algorithms, such as a simulated annealing algorithms, will outweigh the cost of not analyzing the individual terms in the summation. The second approach is to adapt a local least-squares algorithm to the global prob-

lem. Here one can exploit the superior efficiency of the least-squares algorithm.

Our experience indicates that the second approach of treating the problem as a least-squares problem is considerably more efficient. This is probably related to the fact that we are now using up to 200 properties for the least-squares summation, which is considerably more than have been previously used. We have developed an efficient global optimization algorithm by adapting a local least-squares algorithm, the Marquardt-Levenberg algorithm,¹⁶ to the global problem. It involves feeding successive sets of parameters $\{s_i\}$ to the Marquardt-Levenberg algorithm, which finds the local minimum for each set of parameters. Each successive set is chosen with a random distribution from the best set found from all the previous local optimizations. The random distribution is dependent on a scalar “distance” s defined by

$$s = \sqrt{\frac{1}{N_s} \sum_i \left(\frac{s_{next}^i - s_{best}^i}{s_{scale}^i} \right)^2}, \quad (A2)$$

where s_{scale} is the characteristic scale of each parameter. A value s is assigned using a random exponential distribution. The next set of parameters s_{next} to be fed to the Marquardt-Levenberg algorithm can then be constructed from the best parameters s_{best} and the random distance s .

The explicit algorithm for s_{next}^i is given by

$$s_{next}^i = s_{best}^i + \frac{-s_{global} \ln(r_{0,1})}{\sqrt{\frac{\sum_k r_{-1,+1}^k}{N_s}}} r_{-1,+1}^i s_{scale}^i, \quad (A3)$$

where $r_{a,b}$ a random number with a uniform distribution over the interval $[a, b]$, and s_{global} a unitless number which represents the expected range over which the local minima are distributed. A typical value of s_{global} is 0.5, which means that the new parameters will differ from the old parameters by about 50%. Loosely speaking, the random exponential distribution means that the new set of parameters is more likely to be close to the best set of parameters.

Perhaps the most important feature of this random distance algorithm is that successive sets are chosen with regard to the values of the parameters s and without regard to the residual value R . This is in contrast with techniques which interpret the residual R as a type of energy barrier. The highly nonlinear behavior of the residual even in regions where the parameters are reasonable suggests that simulated-annealing-type techniques are not appropriate for these types of optimization problems because the residual barriers are too large. If one does wish to adapt this algorithm to problems where a simulated-annealing-type interpretation is more appropriate, s_{best} can be allowed to “hop” to a local minimum which is not necessarily the best local minimum, with a hopping probability that depends on the difference between two appropriate R values. Indeed, we have used this simulated-annealing-type adaptation at times, and although it certainly adds flair to the algorithm, it does not seem to be useful for our particular problem.

- ¹J. A. Majewski and P. Vogl, Phys. Rev. B **35**, 9666 (1987).
- ²R. E. Cohen, M. J. Mehl, and D. A. Papaconstantopoulos, Phys. Rev. B **50**, 14694 (1994).
- ³M. S. Tang, C. Z. Wang, C. T. Chan, and K. M. Ho, Phys. Rev. B **53**, 979 (1996).
- ⁴A. F. Kohan and G. Ceder, Phys. Rev. B **54**, 805 (1996).
- ⁵Q. Xie and P. Chen, Phys. Rev. B **56**, 5235 (1997).
- ⁶C. M. Goringe, D. R. Bowler, and E. Hernandez, Rep. Prog. Phys. **60**, 1447 (1997).
- ⁷D. A. Papaconstantopoulos, M. J. Mehl, S. C. Erwin, and M. R. Pederson, in *Tight-Binding Approach to Computational Materials Science*, edited by P. E. A. Turchi, A. Gonis, and L. Colombo, MRS Symposia Proceedings No. 491 (Materials Research Society, Pittsburgh, 1998), p. 221; N. Bernstein, M. J. Mehl, D. A. Papaconstantopoulos, N. I. Papanicolaou, M. Z. Bazant, and E. Kaxiras, Phys. Rev. B **62**, 4477 (2000); J. L. Feldman, N. Bernstein, D. A. Papaconstantopoulos, and M. J. Mehl, *ibid.* **70**, 165201 (2004).
- ⁸K. Esfarjani and Y. Kawazoe, J. Phys.: Condens. Matter **10**, 8257 (1998).
- ⁹C. Z. Wang, B. C. Pan, and K. M. Ho, J. Phys.: Condens. Matter **11**, 2043 (1999).
- ¹⁰A. N. Andriotis and M. Menon, Phys. Rev. B **59**, 15942 (1999).
- ¹¹Th. Frauenheim, G. Seifert, M. Elsterner, Z. Hajnal, G. Jungnickel, D. Porezag, S. Suhai, and R. Scholz, Phys. Status Solidi B **217**, 41 (2000).
- ¹²W. M. Foulkes and R. Haydock, Phys. Rev. B **39**, 12520 (1989).
- ¹³R. Hoffmann, J. Chem. Phys. **39**, 1397 (1963).
- ¹⁴R. P. Feynman, Phys. Rev. **56**, 340 (1939).
- ¹⁵J. Ihm, A. Zunger, and M. L. Cohen, J. Phys. C **12**, 4409 (1979); M. T. Yin and M. L. Cohen, Phys. Rev. B **26**, 3259 (1982).
- ¹⁶J. E. Dennis, Jr. and R. B. Schnabel, *Numerical Methods for Unconstrained Optimization and Nonlinear Equation* (Society for Industrial & Applied Mathematics, 1996).
- ¹⁷GAUSSIAN 98 MPW1PW91/cc-pVTZ.
- ¹⁸M. T. Yin and M. L. Cohen, Phys. Rev. B **26**, 5668 (1982).
- ¹⁹W. D. Grobman and D. E. Eastman, Phys. Rev. Lett. **29**, 1508 (1972); W. D. Grobman, D. E. Eastman, and J. E. Freeouf, Phys. Rev. B **12**, 405 (1975).
- ²⁰L. Ley, S. Kowalczyk, R. Pollack, and D. A. Shirley, Phys. Rev. Lett. **29**, 1088 (1972).
- ²¹W. E. Spicer and R. Eden, in *Proceedings of the Ninth International Conference of the Physics of Semiconductors* (Nauka, Leningrad, 1968), Vol. 1, p. 61.
- ²²Th. Frauenheim, F. Weich, Th. Kohler, S. Uhlmann, D. Porezag, and G. Seifert, Phys. Rev. B **52**, 11492 (1995); P. Blaudeck, Th. Frauenheim, D. Porezag, G. Seifert, and E. Fromm, J. Phys.: Condens. Matter **C4**, 6389 (1992).
- ²³M. Menon and K. R. Subbaswamy, Phys. Rev. B **55**, 9231 (1997); **47**, 12754 (1993); **50**, 11577 (1994).
- ²⁴N. Bernstein and E. Kaxiras, Phys. Rev. B **56**, 10488 (1997).
- ²⁵Kai-Ming Ho, Alexander A. Shvartsburg, Bicaï Pan, Zhong-Yi Lu, Cai-Zhuang Wang, Jacob G. Wacker, James L. Fye, and Martin F. Jarrold, Nature (London) **392**, 582 (1998).
- ²⁶J. Song, S. E. Ulloa, and D. A. Drabold, Phys. Rev. B **53**, 8042 (1996).
- ²⁷E. Kaxiras and K. Jackson, Phys. Rev. Lett. **71**, 727 (1993).
- ²⁸L. Mitas, J. C. Grossman, I. Stich, and J. Tobik, Phys. Rev. Lett. **84**, 1479 (2000).
- ²⁹O. F. Sankey and D. J. Niklewski, Phys. Rev. B **40**, 3979 (1989); A. A. Demkov, J. Ortega, O. F. Sankey, and M. P. Grumbach, *ibid.* **52**, 1618 (1995).
- ³⁰J. E. Northrup, Phys. Rev. B **47**, 10032 (1993).
- ³¹Z. Zhu, N. Shima, and M. Tsukada, Phys. Rev. B **40**, 11868 (1989).
- ³²V. Milman, S. J. Pennycook, and D. E. Jesson, Thin Solid Films **272**, 375 (1996).
- ³³C. M. Wei, H. Huang, S. Y. Tong, G. S. Glander, and M. B. Webb, Phys. Rev. B **42**, 11284 (1990).
- ³⁴K. Cho and E. Kaxiras, Europhys. Lett. **39**, 287 (1997); Surf. Sci. **396**, L261 (1998).
- ³⁵Kunio Takayanagi, Yasumasa Tanishiro, Shigeki Takahashi, and Masaetsu Takahashi, Surf. Sci. **164**, 367 (1985); K. Takayanagi, Y. Tanishiro, M. Takahashi, and S. Takahashi, J. Vac. Sci. Technol. A **3**, 1502 (1985).
- ³⁶C. M. Chang and C. M. Wei, Phys. Rev. B **67**, 033309 (2003).
- ³⁷T. Sato, S. Kitamura, and M. Iwatsuki, J. Vac. Sci. Technol. A **18**, 960 (2000).
- ³⁸T. Sato, S. Kitamura, and M. Iwatsuki, Surf. Sci. **445**, 130 (2000).
- ³⁹I.-S. Hwang, M.-S. Ho, and T. T. Tsong, Phys. Rev. Lett. **83**, 120 (1999).
- ⁴⁰A. Tchernatinsky, C. Leahy, D. Migas, M. Yu, C. S. Jayanthi, and S. Y. Wu, Bull. Am. Phys. Soc. **50**, 1265 (2005).
- ⁴¹S. Y. Wu, C. S. Jayanthi, C. Leahy, and M. Yu, *Handbook of Materials Modeling*, edited by S. Yip (Springer, 2005), p. 2935.
- ⁴²Jean-Yves Raty, Giulia Galli, C. Bostedt, Tony W. van Buuren, and Louis J. Terminello, Phys. Rev. Lett. **90**, 037401 (2003).